THE JOURNAL OF PHYSICAL CHEMISTRY LETTERS
A JOURNAL OF THE AMERICAN CHEMICAL SOCIETY

pubs.acs.org/JPCL

Letter

Strong Coupling in Infrared Plasmonic Cavities

Monosij Mondal, Alexander Semenov, Maicol A. Ochoa, and Abraham Nitzan*

Cite This: J. Phys. Chem. Lett. 2022, 13, 9673−9678

Read Online

ACCESS | Metrics & More | Article Recommendations | Supporting Information

ABSTRACT: Controlling molecular spectroscopy and even chemical behavior in a cavity environment is a subject of intense experimental and theoretical interest. In Fabry−Pérot cavities, strong (radiation−matter) coupling phenomena without an intense radiation field often rely on the number of chromophore molecules collectively interacting with a cavity mode. For plasmonic cavities, the cavity field−matter coupling can be strong enough to manifest strong coupling involving even a single molecule. To this end, infrared plasmonic cavities can be particularly useful in understanding vibrational strong coupling. Here we present a procedure for estimating the radiation−matter coupling and, equivalently, the mode volume as well as the mode lifetime and quality factor for plasmonic cavities of arbitrary shapes and use it to estimate these quantities for infrared cavities of two particularly relevant geometries comprising several n-doped semiconductors. Our calculations demonstrate very high field confinement and low mode volumes of these cavities despite having relatively low quality factors, which is often the case for plasmonic cavities.

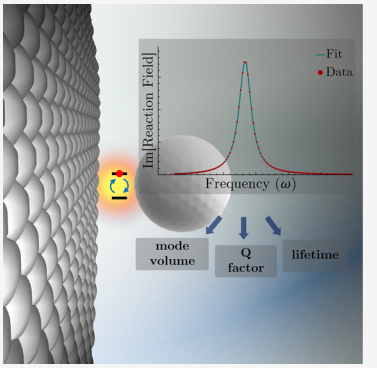

Strong interactions of material excitations with a cavity vacuum electromagnetic field can lead to the formation of hybrid polaritonic states, causing potentially drastic modifications in spectroscopic features,[1−5] energy and charge transfer properties,[6−15] and chemical reactivity.[16−26] Vibrational strong coupling (VSC), manifested by the formation of polaritons when a collective vibrational mode of molecules strongly couples with a cavity mode, has drawn much attention of late. While Fabry−Pérot cavities are often used for such experiments, the latest advancements in micro- and nanofabrication have enabled the construction of highly confined infrared plasmonic cavities[27−32] capable of achieving a large vacuum electromagnetic field. Such cavities (especially mid-IR) can be instrumental in understanding VSC and developing its applications. Plasmonic nanocavities, despite their low quality factors and high ohmic losses, can achieve high field confinement with a subwavelength effective mode volume,[33−35] making it possible to realize strong coupling down to a single- or a few-molecule level.[36] The practical realization of strong coupling is identified as the observation of distinct polariton peaks separated by the so-called Rabi splitting. A necessary condition to achieve this is $2U/\Gamma > 1$, where, in the context of a molecule in a plasmonic cavity, U is the plasmon−molecule coupling and Γ is the width associated with the radiative and nonradiative relaxations of a single molecular vibronic transition, including effects on them induced by the metal. Achieving a large coupling strength while minimizing dissipation is therefore imperative. To assess the performance of plasmonic cavities, we need to examine the effects of the cavity geometry and material properties on the local manifestation of light−matter coupling as expressed by the collective optical response (such as but not limited to[37] plasmon excitations, local field enhancement, and radiative and nonradiative relaxation of the molecular excitations).

Recently,[38] following Gersten and Nitzan,[39] we have studied the interplay between field enhancement and dissipation and their dependence on the geometry and the composition of (metal) nanoparticle−molecule interfaces with regard to the realization of strong coupling in such structures. We observe that the coupling can vary within a range of several orders of magnitude depending on the nanoparticle−molecule distance, the molecular orientation, and the curvature of the nanoparticle surface. Interestingly, we have found that when Γ is dominated by the molecule−metal interaction, the condition $2U/\Gamma > 1$ is often satisfied.

Here we extend this method[38] to investigate strong coupling in plasmonic cavities, particularly emphasizing structures and materials that support infrared cavity modes. Although vacuum-field effects are quantum in nature, we show that the strength of light−matter interaction, commonly expressed in terms of an effective cavity volume (or as done here by a coupling parameter M that we define shortly), can be estimated from classical calculations. In these structures, one often encounters the need to consider the vastly different length scales which make the numerical calculation of the optical response expensive. In the present work, therefore, we have considered two cavity configurations (Figure 1) that can be addressed analytically

Received: July 25, 2022
Accepted: September 21, 2022

https://doi.org/10.1021/acs.jpclett.2c02304
J. Phys. Chem. Lett. 2022, 13, 9673−9678

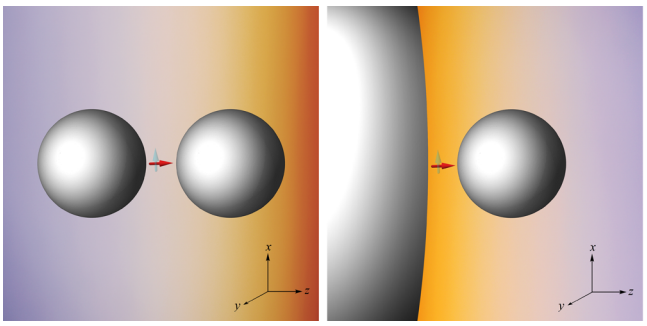

Figure 1. Schematic representation of a plasmonic cavity formed by the near contact of (a) two identical dielectric nanospheres and (b) two nanospheres with one having a radius larger than the other so that the configuration approximates sphere-on-plane geometry. A molecular dipole at the center of the gap between the nanoparticles, orienting parallel or perpendicular to the cavity (z) axis, is driving the cavity in both (a) and (b).

and are frequently fabricated in plasmonic cavity experiments: a spherical nanoparticle dimer and a (spherical) nanoparticle-on-mirror (NPoM) made of several doped semiconductor materials. We calculate relevant physical properties, namely, the coupling parameter M, the effective mode volume Ω_{cav}, the plasmon width γ, and the quality factor Q for these cavities. We will briefly describe the theory before presenting the results.

THEORETICAL CONSIDERATIONS

Here we consider a molecule inside an optical cavity of a geometry of choice (Figure 1). We assume that the cavity is characterized by distinct optical resonances (plasmonic cavity modes) and limit ourselves to near-resonance between the molecular transition and such a cavity mode. (The plasmonic response of a given metal nanostructure is usually characterized by many resonances that may overlap. Here we assume that the response to a driving dipole of a distinct frequency ω_0 is dominated by a single resonance.) The molecular dipole, oriented parallel or perpendicular to the cavity axis z, is driving the system. To evaluate the electromagnetic response to this driving and thereby the cavity properties, we consider a system Hamiltonian $\hat{H} = \hat{H}_M + \hat{H}_C + \hat{H}_{MC}$. Here, the molecular (M) Hamiltonian $\hat{H}_M$ with two levels 1 and 2 is given by $\hat{H}_M = E_1|1\rangle\langle 1| + E_2|2\rangle\langle 2|$, and with the assumption that the interaction of the molecule with the cavity field is dominated by a single cavity mode, the cavity (C)-field Hamiltonian is $\hat{H}_C = \hbar\omega_0\hat{a}^\dagger\hat{a}$ where $\hat{a}$ and $\hat{a}^\dagger$ are the mode annihilation and creation operators and ω_0 is the mode frequency. The interaction is given by $\hat{H}_{MC} = -iM[\mu_{12}|1\rangle\langle 2| + \mu_{21}|2\rangle\langle 1|](\hat{a} - \hat{a}^\dagger)$, with μ_{12} being the transition dipole moment between 1 and 2. The coupling parameter M depends, in general, on the oscillator position and orientation inside the cavity, the cavity geometry, and the material composition. In vacuum, M is given by $M = \sqrt{\frac{\hbar\omega}{2\epsilon_0\Omega}}$ where ω is the mode frequency and Ω is the cavity volume. In order to connect our cavity model in Figure 1 to this Hamiltonian, we need to calculate the parameter M for the desired geometry. The effective cavity volume Ω_{cav} is defined in this context from the expression of M in vacuum: $\Omega_{cav} = \hbar\omega_0/(2\epsilon_0 M^2)$.

The coupling parameter M is the same in classical, semiclassical, and quantum electrodynamics. We can therefore evaluate this parameter by considering the cavity response to classical driving. To this end, we replace the molecular transition dipole μ_{12} by a classical point dipole $\mu(t)$, oscillating at frequency ω_0, that drives the plasmonic cavity mode while keeping the quantum character of the latter. (This is not a necessity[38] but serves to simplify the language in the derivation shown in S1 in the Supporting Information.) To include the dissipation ocurring at the dielectric boundaries as well as emission to the far field, the Hamiltonian is supplemented by linear coupling terms to a Markovian (white) boson bath. Therefore, $\hat{H}$ describes a quantum oscillator, driven by an oscillating classical field of amplitude $M\mu(t)$, interacting with a bosonic bath represented by boson annihilation and creation operators $\hat{b}_j$, $\hat{b}_j^\dagger$:

$$\hat{H} = \hbar\omega_0\hat{a}^\dagger\hat{a} - i\mu(t)\,M(\hat{a} - \hat{a}^\dagger) + \hbar\sum_j \omega_j\hat{b}_j^\dagger\hat{b}_j + \hbar\sum_j u_j(\hat{a}^\dagger + \hat{a})(\hat{b}_j^\dagger + \hat{b}_j) \quad (1)$$

Here, $iM(\hat{a} - \hat{a}^\dagger)$ represents the electric field operator at the position and in the direction of the driving dipole. In section S1 in the Supporting Information, we describe the evaluation of the system response to the classical driving in detail. Under the rotating wave approximation, this calculation yields the steady-state expectation value of this reaction field, $E_{RF}(\omega)$,

$$Re[E_{RF}(\omega)] = \frac{M^2\mu(\tilde{\omega}_0 - \omega)}{\hbar[(\omega - \tilde{\omega}_0)^2 + (\gamma/2)^2]} \quad (2)$$

$$Im[E_{RF}(\omega)] = \frac{M^2\mu\gamma}{2\hbar[(\omega - \tilde{\omega}_0)^2 + (\gamma/2)^2]} \quad (3)$$

where $\tilde{\omega}_0 = \omega_0 + \delta\omega$and $\delta\omega$ and γ represent the plasmon frequency shift and width (both taken to be frequency-independent), respectively. By evaluating $E_{RF}(\omega)$ in the vicinity of a cavity resonance, we can extract the parameters M (and also Ω_{cav}), $\tilde{\omega}_0$, and γ by fitting to eqs 2 and 3. For the cavity structures considered in this work, the plasmon response to the driving dipole and thereby the projection of the reaction field in the dipole direction can be obtained semianalytically under the electrostatic (long-wavelength) approximation.[38] Finally, the quality factor Q of the cavity is obtained as $Q = \tilde{\omega}_0/\gamma$.

RESULTS

In Table 1 and Table S1 in the Supporting Information, we report these parameters for cavities with a spherical nanoparticle dimer and NPoM configurations made of several n-doped semiconductors that are known to show plasmonic resonances in THz to the mid-IR range.[29] Doped conducting metal oxides (e.g., Al:ZnO, Ga:ZnO, and Ga:CdO) allow great tunability of plasmonic properties by altering the dopant concentration. For the sake of reference, we also include silver and gold, materials frequently used in plasmonic cavities supporting higher-frequency modes. For the doped semiconductors used here, the resonance frequencies are much smaller than interband transition frequencies. As a result, a simple dielectric response function, such as the Drude function, works well near plasmon frequencies.[40] In the frequency domain, the dielectric response of the plasmonic structure, $\epsilon_d(\omega)$, is given by

https://doi.org/10.1021/acs.jpclett.2c02304
J. Phys. Chem. Lett. 2022, 13, 9673−9678

Table 1. Evaluated Quantities for Cavities Formed by the Near Contact of Two Dielectric Nanospheres of Radii 10 and 2000 nm with a Gap of 1 nm in between (Approximating Sphere-on-Plane Geometry): Parallel and Perpendicular Orientations of the Source Dipole

cavity material		■ → ●	■ ↑ ●
AZO (Al:ZnO) (2 wt %)	M (V/m)	9.426×10^8	6.80×10^8
$\varepsilon_b = 3.5402$	$\tilde{\omega}_0$ (eV)	0.809	0.831
$\omega_p = 0.929$ eV	γ (eV)	0.0513	0.0577
$\Gamma = 0.045$ eV[41]	Ω_{cav} (nm^3)	8.24	16.24
	Q	15.77	14.39
GZO (Ga:ZnO) (4 wt %)	M (V/m)	1.15×10^9	7.56×10^8
$\varepsilon_b = 3.2257$	$\tilde{\omega}_0$ (eV)	0.944	0.982
$\omega_p = 1.108$ eV	γ (eV)	0.1338	0.1334
$\Gamma = 0.123$ eV[41]	Ω_{cav} (nm^3)	6.35	15.54
	Q	7.055	7.36
ITO (10 wt %)	M (V/m)	1.08×10^9	6.73×10^8
$\varepsilon_b = 3.528$	$\tilde{\omega}_0$ (eV)	0.810	0.847
$\omega_p = 0.948$ eV	γ (eV)	0.165	0.1600
$\Gamma = 0.155$ eV[41]	Ω_{cav} (nm^3)	6.25	16.86
	Q	4.91	5.29
n-GaAs (Si dopant)	M (V/m)	1.95×10^8	1.07×10^8
carrier concentration	$\tilde{\omega}_0$ (eV)	0.060	0.062
$(0.8-4) \times 10^{18}$ cm^{-3}	γ (eV)	0.00994	0.0092
$\varepsilon_b = 11.58$, $\omega_p = 0.06441$ eV	Ω_{cav} (nm^3)	14.39	48.20
$\Gamma = 0.00927$ eV[42]	Q	6.09	6.67
n-InP (S dopant)	M (V/m)	2.52×10^8	1.42×10^8
carrier concentration	$\tilde{\omega}_0$ (eV)	0.091	0.094
$(0.8-8) \times 10^{18}$ cm^{-3}	γ (eV)	0.0106	0.0094
$\varepsilon_b = 10.01$, $\omega_p = 0.09779$ eV	Ω_{cav} (nm^3)	12.99	42.00
$\Gamma = 0.00927$ eV[42]	Q	8.65	9.93
n-InSb (Te dopant)	M (V/m)	1.41×10^8	8.04×10^7
carrier concentration	$\tilde{\omega}_0$ (eV)	0.045	0.046
$(0.19-0.50) \times 10^{18}$ cm^{-3}	γ (eV)	0.00281	0.00255
$\varepsilon_b = 15.68$, $\omega_p = 0.0468711$ eV	Ω_{cav} (nm^3)	20.48	63.81
$\Gamma = 0.00248$ eV[42]	Q	16.02	17.89
gold	M (V/m)	1.26×10^9	8.08×10^8
$\varepsilon_b = 9.5$	$\tilde{\omega}_0$ (eV)	2.74	2.78
$\omega_p = 2.903$ eV	γ (eV)	0.0922	0.086
$\Gamma = 0.069$ eV[43]	Ω_{cav} (nm^3)	15.56	38.51
	Q	29.70	32.41
silver	M (V/m)	1.51×10^9	9.47×10^8
$\varepsilon_b = 8.926$	$\tilde{\omega}_0$ (eV)	3.64	3.70
$\omega_p = 3.8776$ eV	γ (eV)	0.2231	0.2181
$\Gamma = 0.203$ eV[44]	Ω_{cav} (nm^3)	14.48	37.36
	Q	16.30	16.97

$\epsilon_d(\omega) = \epsilon_b\left[1 - \frac{\omega_p^2}{\omega(\omega + i\Gamma)}\right]$, where ε_b is the background permittivity from the bound electrons, ω_p is the plasma frequency of the bulk, and Γ is a phenomenological damping constant. These parameters for all cavity materials are provided in Table 1. We note that more accurate representations of $\varepsilon_d(\omega)$, needed to describe interband transitions, can be obtained by augmenting the Drude model with Lorentzian functions; however, the Drude model is known to work reasonably well for the materials selected in our chosen frequency range. For medium embedding, the nanoparticles, and the molecule, the dielectric constant, ε_s, is set to 1. We choose the particular plasmonic cavity geometry formed by the near contact of a 10-nm-radius nanosphere to another nanosphere of 2000 nm radius (the latter much larger than the earlier) with a 1 nm gap in between, therefore providing a good representation of a nanoparticle-on-mirror (NPoM, here sphere-on-plane) configuration. Here and in all calculations in this report, the driving dipole is located on the cavity axis in the center of the gap. We have considered both parallel and perpendicular (to the cavity axis z) orientations of the dipole. In Table S1 in the Supporting Information, we include results for the nanosphere dimer, each of radius 10 nm with a 1 nm gap in between for both parallel and perpendicular orientations of the source dipole (also located in the center of the gap).

For all of the materials considered here, as seen in Table 1, the appreciable magnitude of M is obtained for the structures, with several substrates giving remarkably small cavity volumes of ~10 nm^3. They are, however, characterized by relatively low quality factors. Plasmonic cavities are usually marked by low quality factors,[45−47] owing to intrinsic losses, radiation, and scattering. The plasmon frequency and the plasmon width are rather insensitive to the orientation of the source dipole. For example, for the n-InP structure we find $\tilde{\omega}_0 = 0.091$ eV and $\gamma = 0.0106$ eV

https://doi.org/10.1021/acs.jpclett.2c02304
J. Phys. Chem. Lett. 2022, 13, 9673−9678

in the parallel orientation and $\tilde{\omega}_0 = 0.094$ eV and $\gamma = 0.0094$ eV in the perpendicular orientation. A similar trend is observed for the nanoparticle dimer configurations in Table S1 in the Supporting Information. Moreover, as seen from Figure S2a,b in the Supporting Information, the plasmon frequency and the width remain practically unchanged even with a varying gap size (within the range of our study) between two nanospheres of 2000 and 10 nm radii. (The plasmonic response of a given metal nanostructure is usually characterized by many resonances that may overlap. Here we assume that the response to a driving dipole of a distinct frequency ω_0 is dominated by a single resonance.) We do not consider gap sizes of less than 1 nm (or equivalently a molecule−nanoparticle surface distance of less than 0.5 nm) as we disregard quantum mechanical effects, such as tunneling, in our calculations. From these, we can predict that the gap size cannot be used as a robust tuning parameter for $\tilde{\omega}_0$ or γ. Alternative ways to tune the spectral response of these cavities, e.g., doping levels and other geometric characteristics, need further study.

In contrast to the plasmon frequency and width, the coupling parameter M (and therefore, obviously, the effective mode volume, Ω_{cav}) is very sensitive to the cavity gap size. In Figure 2,

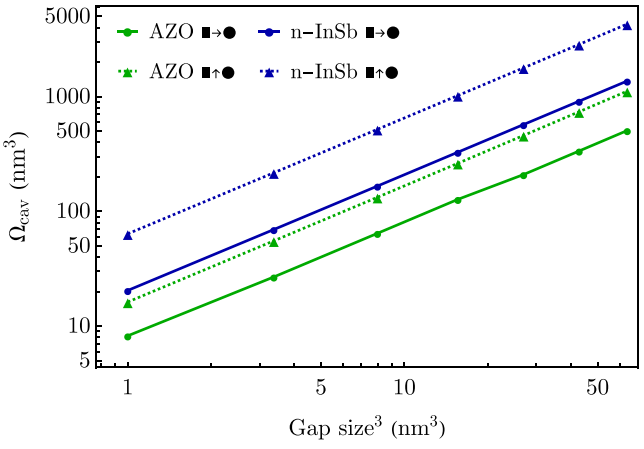

Figure 2. Effective mode volume, Ω_{cav}, as functions of the cube of the gap size between two nanospheres of radii 2000 and 10 nm (approximating sphere-on-plane geometry): parallel and perpendicular orientations of the source dipole in the center of the gap. Shown on logarithmic scales.

we plot Ω_{cav} for the nanoparticle-on-mirror configuration of AZO and n-InSb by considering both parallel and perpendicular orientations of the dipole (we report corresponding M values in Figure S1 in the Supporting Information for the sake of completeness) for a cavity formed by two nanospheres of 2000 and 10 nm radii with varying gap sizes (which we plot as functions of the third power of the gap size). With increasing gap size, the mode volume rapidly increases for both materials and both orientations of the dipole. For example, with parallel orientation in the AZO cavity, changing the gap size from 1 to 2 nm results in a change of Ω_{cav} from 8.2 to 64.5 nm^3. Specifically, we observe that the effective mode volume, as defined by $\Omega_{cav} = \hbar\omega_0/(2\varepsilon_0 M^2)$, is linearly related to (gap size)^3. It is interesting that similar to Fabry−Pérot cavities, even in these plasmonic structures, the cavity volume mostly reflects the gap size while being rather insensitive to the particle size: changing the radius of one nanosphere from 5 to 25 nm while keeping the other constant at 2000 nm with a fixed gap size (either 1 nm, as shown in Figure S3 in the SI, or 2 nm) has practically no effect on Ω_{cav}. However, the resonance frequency of a plasmonic cavity of certain gap size is very different from what would be inferred from a Fabry−Pérot cavity of the same gap size between the mirrors. We also note that for the same cavity material and the range of the gap size considered here, the mode volume for the parallel orientation is significantly lower than the perpendicular orientation.

In summary, we have introduced a method for computing the cavity field−molecule coupling and the corresponding mode volume that can be used for a molecule inside plasmonic cavities of arbitrary geometries where the needed input is the response to a driving dipole near a distinct peak. Here we have particularly considered configurations (the near contact of two dielectric spheres, including the limit when one of the spheres is larger enough relative to the other to effectively act as a planar surface) for which we can use analytical results (in the long-wavelength approximation) to evaluate the relevant cavity parameters, although more complex geometries can be considered numerically with standard FDTD codes. We have focused on structures, with doped semiconductors as building materials, that are characterized by their plasmonic response in the infrared range even under confinements on the order of 1 nm, albeit with relatively low quality factors. We have observed that similar to Fabry−Pérot cavities, the effective cavity volume in the structures investigated is still dominated by the geometric volume of the plasmonic cavities. Such cavities may provide a useful playground for future studies of the vibrational strong coupling phenomenon involving one or a few molecules.

■ ASSOCIATED CONTENT

Supporting Information

The Supporting Information is available free of charge at https://pubs.acs.org/doi/10.1021/acs.jpclett.2c02304.

Derivation of the reaction field; table of cavity parameters for nanoparticle dimer configuration; trends in the coupling parameter, plasmon frequency, and plasmon width as functions of the cavity gap size; effective mode volume as a function of nanoparticle size; and an example of fitting the reaction field to extract the cavity parameters (PDF)

■ AUTHOR INFORMATION

Corresponding Author

Abraham Nitzan − *Department of Chemistry, University of Pennsylvania, Philadelphia, Pennsylvania 19104, United States; School of Chemistry, Tel Aviv University, Tel Aviv 69978, Israel;* orcid.org/0000-0002-8431-0967; Email: anitzan@sas.upenn.edu

Authors

Monosij Mondal − *Department of Chemistry, University of Pennsylvania, Philadelphia, Pennsylvania 19104, United States;* orcid.org/0000-0003-4764-0737

Alexander Semenov − *Department of Chemistry, University of Pennsylvania, Philadelphia, Pennsylvania 19104, United States*

Maicol A. Ochoa − *Department of Chemistry, University of Pennsylvania, Philadelphia, Pennsylvania 19104, United States;* Present Address: Nanoscale Device Characterization Division, National Institute of Standards and Technology, Gaithersburg, Maryland 20899, United

https://doi.org/10.1021/acs.jpclett.2c02304
J. Phys. Chem. Lett. 2022, 13, 9673−9678

States and Department of Chemistry and Biochemistry, University of Maryland, College Park, Maryland 20742, United States

Complete contact information is available at: https://pubs.acs.org/10.1021/acs.jpclett.2c02304

Notes

The authors declare no competing financial interest.

■ ACKNOWLEDGMENTS

This research of A.N. was supported by the U.S. National Science Foundation (grant no. CHE1953701).

■ REFERENCES

(1) Ribeiro, R. F.; Martínez-Martínez, L. A.; Du, M.; Campos-Gonzalez-Angulo, J.; Yuen-Zhou, J. Polariton chemistry: controlling molecular dynamics with optical cavities. *Chemical Science* **2018**, *9*, 6325−6339.

(2) del Pino, J.; Feist, J.; Garcia-Vidal, F. J. Quantum theory of collective strong coupling of molecular vibrations with a microcavity mode. *New J. Phys.* **2015**, *17*, 053040.

(3) Hertzog, M.; Wang, M.; Mony, J.; Börjesson, K. Strong light−matter interactions: a new direction within chemistry. *Chem. Soc. Rev.* **2019**, *48*, 937−961.

(4) Li, T. E.; Cui, B.; Subotnik, J. E.; Nitzan, A. Molecular Polaritonics: Chemical Dynamics Under Strong Light−Matter Coupling. *Annu. Rev. Phys. Chem.* **2022**, *73*, 43−71.

(5) Garcia-Vidal, F. J.; Ciuti, C.; Ebbesen, T. W. Manipulating matter by strong coupling to vacuum fields. *Science* **2021**, *373*, No. eabd0336.

(6) Delor, M.; Scattergood, P. A.; Sazanovich, I. V.; Parker, A. W.; Greetham, G. M.; Meijer, A. J.; Towrie, M.; Weinstein, J. A. Toward control of electron transfer in donor-acceptor molecules by bond-specific infrared excitation. *Science* **2014**, *346*, 1492−1495.

(7) Coles, D. M.; Somaschi, N.; Michetti, P.; Clark, C.; Lagoudakis, P. G.; Savvidis, P. G.; Lidzey, D. G. Polariton-mediated energy transfer between organic dyes in a strongly coupled optical microcavity. *Nat. Mater.* **2014**, *13*, 712−719.

(8) Orgiu, E.; George, J.; Hutchison, J. A.; Devaux, E.; Dayen, J. F.; Doudin, B.; Stellacci, F.; Genet, C.; Schachenmayer, J.; Genes, C.; et al. Conductivity in organic semiconductors hybridized with the vacuum field. *Nat. Mater.* **2015**, *14*, 1123−1129.

(9) Hagenmüller, D.; Schachenmayer, J.; Schütz, S.; Genes, C.; Pupillo, G. Cavity-Enhanced Transport of Charge. *Phys. Rev. Lett.* **2017**, *119*, 223601.

(10) Groenhof, G.; Toppari, J. J. Coherent Light Harvesting through Strong Coupling to Confined Light. *J. Phys. Chem. Lett.* **2018**, *9*, 4848−4851.

(11) Duan, H.-G.; Nalbach, P.; Miller, R. J. D.; Thorwart, M. Ultrafast Energy Transfer in Excitonically Coupled Molecules Induced by a Nonlocal Peierls Phonon. *J. Phys. Chem. Lett.* **2019**, *10*, 1206−1211.

(12) Rozenman, G. G.; Akulov, K.; Golombek, A.; Schwartz, T. Long-Range Transport of Organic Exciton-Polaritons Revealed by Ultrafast Microscopy. *ACS Photonics* **2018**, *5*, 105−110.

(13) Xiang, B.; Ribeiro, R. F.; Du, M.; Chen, L.; Yang, Z.; Wang, J.; Yuen-Zhou, J.; Xiong, W. Intermolecular vibrational energy transfer enabled by microcavity strong light−matter coupling. *Science* **2020**, *368*, 665−667.

(14) Li, T. E.; Nitzan, A.; Subotnik, J. E. Collective Vibrational Strong Coupling Effects on Molecular Vibrational Relaxation and Energy Transfer: Numerical Insights via Cavity Molecular Dynamics Simulations. *Angew. Chem., Int. Ed.* **2021**, *133*, 15661−15668.

(15) Cao, J.Generalized resonance energy transfer theory: Applications to vibrational energy flow in optical cavities. *arXiv***2022**, 2201.12117.

(16) Thomas, A.; George, J.; Shalabney, A.; Dryzhakov, M.; Varma, S. J.; Moran, J.; Chervy, T.; Zhong, X.; Devaux, E.; Genet, C.; et al. Ground-State Chemical Reactivity under Vibrational Coupling to the Vacuum Electromagnetic Field. *Angew. Chem., Int. Ed.* **2016**, *55*, 11462.

(17) Munkhbat, B.; Wersäll, M.; Baranov, D. G.; Antosiewicz, T. J.; Shegai, T. Suppression of photo-oxidation of organic chromophores by strong coupling to plasmonic nanoantennas. *Science Advances* **2018**, *4*, No. eaas9552.

(18) Thomas, A.; Lethuillier-Karl, L.; Nagarajan, K.; Vergauwe, R. M.; George, J.; Chervy, T.; Shalabney, A.; Devaux, E.; Genet, C.; Moran, J.; et al. Tilting a ground-state reactivity landscape by vibrational strong coupling. *Science* **2019**, *363*, 615−619.

(19) Galego, J.; Climent, C.; Garcia-Vidal, F. J.; Feist, J. Cavity Casimir-Polder Forces and Their Effects in Ground-State Chemical Reactivity. *Physical Review X* **2019**, *9*, 021057.

(20) Campos-Gonzalez-Angulo, J. A.; Ribeiro, R. F.; Yuen-Zhou, J. Resonant catalysis of thermally activated chemical reactions with vibrational polaritons. *Nat. Commun.* **2019**, *10*, 4685.

(21) Pang, Y.; Thomas, A.; Nagarajan, K.; Vergauwe, R. M. A.; Joseph, K.; Patrahau, B.; Wang, K.; Genet, C.; Ebbesen, T. W. On the Role of Symmetry in Vibrational Strong Coupling: The Case of Charge-Transfer Complexation. *Angew. Chem., Int. Ed.* **2020**, *132*, 10522−10526.

(22) Fregoni, J.; Granucci, G.; Persico, M.; Corni, S. Strong Coupling with Light Enhances the Photoisomerization Quantum Yield of Azobenzene. *Chem.* **2020**, *6*, 250−265.

(23) Thomas, A.; Jayachandran, A.; Lethuillier-Karl, L.; Vergauwe, R. M. A.; Nagarajan, K.; Devaux, E.; Genet, C.; Moran, J.; Ebbesen, T. W. Ground state chemistry under vibrational strong coupling: dependence of thermodynamic parameters on the Rabi splitting energy. *Nanophotonics* **2020**, *9*, 249−255.

(24) Yang, P.-Y.; Cao, J. Quantum Effects in Chemical Reactions under Polaritonic Vibrational Strong Coupling. *J. Phys. Chem. Lett.* **2021**, *12*, 9531−9538.

(25) Sau, A.; Nagarajan, K.; Patrahau, B.; Lethuillier-Karl, L.; Vergauwe, R. M. A.; Thomas, A.; Moran, J.; Genet, C.; Ebbesen, T. W. Modifying Woodward−Hoffmann Stereoselectivity Under Vibrational Strong Coupling. *Angew. Chem., Int. Ed.* **2021**, *133*, 5776−5781.

(26) Dunkelberger, A. D.; Simpkins, B. S.; Vurgaftman, I.; Owrutsky, J. C. Vibration-Cavity Polariton Chemistry and Dynamics. *Annu. Rev. Phys. Chem.* **2022**, *73*, 429−451.

(27) Stanley, R. Plasmonics in the mid-infrared. *Nat. Photonics* **2012**, *6*, 409−411.

(28) Brar, V. W.; Jang, M. S.; Sherrott, M.; Lopez, J. J.; Atwater, H. A. Highly confined tunable mid-infrared plasmonics in graphene nanoresonators. *Nano Lett.* **2013**, *13*, 2541−2547.

(29) Zhong, Y.; Malagari, S. D.; Hamilton, T.; Wasserman, D. Review of mid-infrared plasmonic materials. *Journal of Nanophotonics* **2015**, *9*, 093791.

(30) Hugall, J. T.; Singh, A.; Van Hulst, N. F. Plasmonic Cavity Coupling. *ACS Photonics* **2018**, *5*, 43−53.

(31) Taliercio, T.; Biagioni, P. Semiconductor infrared plasmonics. *Nanophotonics* **2019**, *8*, 949−990.

(32) Frisk Kockum, A.; Miranowicz, A.; De Liberato, S.; Savasta, S.; Nori, F. Ultrastrong coupling between light and matter. *Nature Reviews Physics* **2019**, *1*, 19−40.

(33) Santhosh, K.; Bitton, O.; Chuntonov, L.; Haran, G. Vacuum Rabi splitting in a plasmonic cavity at the single quantum emitter limit. *Nat. Commun.* **2016**, *7*, ncomms11823.

(34) Xiang, B.; Xiong, W. Molecular vibrational polariton: Its dynamics and potentials in novel chemistry and quantum technology. *J. Chem. Phys.* **2021**, *155*, 050901.

(35) Itoh, T.; Yamamoto, Y. S. Between plasmonics and surface-enhanced resonant Raman spectroscopy: toward single-molecule strong coupling at a hotspot. *Nanoscale* **2021**, *13*, 1566−1580.

(36) Chikkaraddy, R.; De Nijs, B.; Benz, F.; Barrow, S. J.; Scherman, O. A.; Rosta, E.; Demetriadou, A.; Fox, P.; Hess, O.; Baumberg, J. J. Single-molecule strong coupling at room temperature in plasmonic nanocavities. *Nature* **2016**, *535*, 127−130.

(37) Kivshar, Y. The Rise of Mie-tronics. *Nano Lett.* **2022**, *22*, 3513−3515.

(38) Mondal, M.; Ochoa, M. A.; Sukharev, M.; Nitzan, A. Coupling, lifetimes, and "strong coupling" maps for single molecules at plasmonic interfaces. *J. Chem. Phys.* **2022**, *156*, 154303.
(39) Gersten, J.; Nitzan, A. Spectroscopic properties of molecules interacting with small dielectric particles. *J. Chem. Phys.* **1981**, *75*, 1139−1152.
(40) Khamh, H.; Sachet, E.; Kelly, K.; Maria, J.-P.; Franzen, S. As good as gold and better: conducting metal oxide materials for mid-infrared plasmonic applications. *Journal of Materials Chemistry C* **2018**, *6*, 8326−8342.
(41) Naik, G. V.; Shalaev, V. M.; Boltasseva, A. Alternative Plasmonic Materials: Beyond Gold and Silver. *Adv. Mater.* **2013**, *25*, 3264−3294.
(42) Chochol, J.; Postava, K.; Čada, M.; Vanwolleghem, M.; Mičica, M.; Halagačka, L.; Lampin, J.-F.; Pištora, J. Plasmonic behavior of III-V semiconductors in far-infrared and terahertz range. *Journal of the European Optical Society-Rapid Publications* **2017**, *13*, 13.
(43) Oubre, C.; Nordlander, P. J. Plasmonics: Metallic Nanostructures and Their Optical Properties. *SPIE* **2003**, *5221*, 133−143.
(44) Gray, S. K.; Kupka, T. Propagation of light in metallic nanowire arrays: Finite-difference time-domain studies of silver cylinders. *Phys. Rev. B* **2003**, *68*, 045415.
(45) Wang, F.; Harutyunyan, H. Tailoring the quality factors and nonlinear response in hybrid plasmonic-dielectric metasurfaces. *Opt. Express* **2018**, *26*, 120−129.
(46) Chorsi, H. T.; Lee, Y.; Alù, A.; Zhang, J. X. J. Tunable plasmonic substrates with ultrahigh Q-factor resonances. *Sci. Rep.* **2017**, *7*, 15985.
(47) Min, B.; Ostby, E.; Sorger, V.; Ulin-Avila, E.; Yang, L.; Zhang, X.; Vahala, K. High- Q surface-plasmon-polariton whispering-gallery microcavity. *Nature* **2009**, *457*, 455−458.

https://doi.org/10.1021/acs.jpclett.2c02304
J. Phys. Chem. Lett. 2022, 13, 9673−9678